INORGANIC CHEMISTRY FRONTIERS

RESEARCH ARTICLE

View Article Online
View Journal | View Issue

Cite this: *Inorg. Chem. Front.*, 2021, **8**, 2611

Magnetic properties of two $Gd^{III}Fe^{III}_4$ metallacrowns and strategies for optimizing the magnetocaloric effect of this topology†

Elvin V. Salerno, [a] Jeff W. Kampf,[a] Vincent L. Pecoraro *[a] and Talal Mallah *[b]

Received 16th February 2021,
Accepted 8th April 2021

DOI: 10.1039/d1qi00207d

rsc.li/frontiers-inorganic

Two Gd^{III} $Fe^{III}4$ metallacrown complexes are presented and analyzed for their magnetic properties. One of these species is newly identified and exhibits a bent ring geometry as opposed to the more conventional flatter conformation of the other. Both complexes are quite similar magnetically, exhibiting antiferromagnetic exchange coupling values *ca.* $J(Fe^{III}–N–O–Fe^{III})$ = −7 cm^{-1} and $J(Gd^{III}–O–Fe^{III})$ = −0.7 cm^{-1}. When analyzed for the molecular magnetocaloric effect, maximum $-\Delta S_m$ values of 7.3 J K^{-1} kg^{-1} at 3 K and at 6.1 J K^{-1} kg^{-1} at 4 K were exhibited. A detailed structural-magnetic correlation is established and an assessment of several similar magnetic metallacrowns with diverse metal combinations is given with regards to their potential magnetocaloric properties. Strategies for improving the magnetocaloric properties within the MetaIn + FeIII4 family of metallacrowns are proposed regarding the ratio between coupling parameters $J(Fe^{III}–N–O–Fe^{III})/J(Metal^{n+}–O–Fe^{III})$.

Introduction

Magnetic materials are pervasive in modern society. These materials provide the basis for a wide range of technological applications such as magnetic data storage,[1] audio speakers,[2] electric power generation,[3] magnetic imaging,[4] and many more.[5] The continued improvement of these technologies depends on an understanding of the origin of magnetic properties and how to control them.

One potential use for magnetic materials is magnetorefrigeration that exploits the magnetocaloric effect (MCE) to cool a system of interest.[6,7] The magnetocaloric effect (MCE) can be described as the change in temperature of a material in response to a changing magnetic field. By controlling heat exchange with the surroundings, and by appropriately cycling the magnetization and demagnetization of a material, a magnetorefrigeration system can be produced.

The MCE is universal to magnetic materials. However, the magnitude of this effect and the temperature region where it is most effective is dependent on the inherent magnetic properties of a given system. While bulk metals tend to have optimal functionality in the higher temperature range (*e.g.* bulk Gd which has maximal MCE around 300 K);[8] in the low temperature cryogenic region (<20 K) and in particular the very low temperature region *ca.* 2 K, paramagnetic based MCE agents (such as GdF_3) have demonstrated an emergence as the most effective materials for this purpose.[9–11]

Molecular magnetic materials have also been studied as low-temperature MCE agents because they can be systematically manipulated by chemical synthetic techniques, allowing for fine-tuning of magnetic properties.[12–14] This allows potential for improving MCE behavior and reducing costs, for example by using tuned Fe^{III} metal centers which are highly abundant and cheap, and have a large spin value (S = 5/2).

While there are at this juncture many 3d,[15–17] 4f[18,19] and mixed 3d–4f[20–22] molecular materials exhibiting a range of MCE properties, among them some with high performance,[23–27] their properties that rely on their structure, on the topology of the exchange coupling between the metal ions, and on the magnitude of the coupling are generally difficult to control. Metallacrowns are a class of molecular complexes with the rare trait that they form common (usually predictable) structural motifs leading to a well-defined spin topology that allows a certain degree of control on the nature of their ground spin state.[28–33] As such, they serve as tunable systems that allow for the evaluation of magnetostructurral correlations between metal centers. These compounds possess the archetypal motif –$[M–N–O]_n$–, where M is a metal ion such

[a]*Department of Chemistry, Willard H. Dow Laboratories, University of Michigan, Ann Arbor, Michigan 48109, USA. E-mail: vlpec@umich.edu*
[b]*Institut de Chimie Moléculaire et des Matériaux d'Orsay, CNRS, Université Paris-Saclay, 91405 Orsay Cedex, France. E-mail: talal.mallah@universite-paris-saclay.fr*

†Electronic supplementary information (ESI) available: X-ray crystallographic parameters, including CIF file and images, and additional magnetic analysis information. CCDC 2034413. For ESI and crystallographic data in CIF or other electronic format see DOI: 10.1039/d1qi00207d

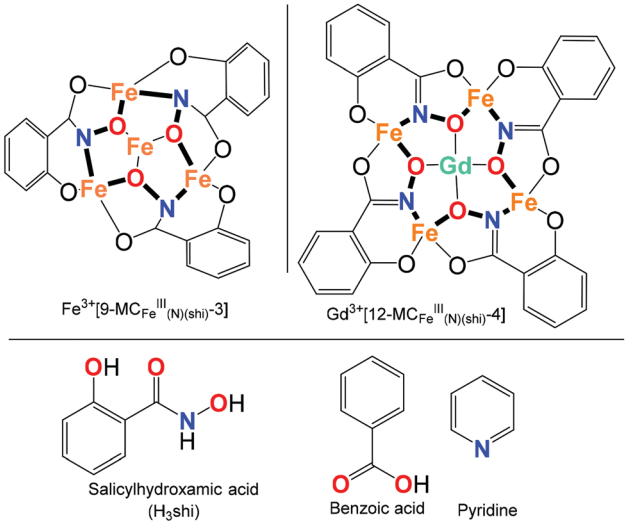

Fig. 1 (Top left) Fe^{III}[9-$MC_{Fe^{III}(N)(shi)}$-3] schematic where the typical metallacrown –[metal–nitrogen–oxygen]$_n$-motif is in bold. This is a typical 9-MC-3 metallacrown. (Top right) Gd^{III}[12-$MC_{Fe^{III}(N)(shi)}$-4] metallacrown, a typical 12-MC-4 metallacrown. (Bottom) Some ligands used in this study. Potential coordinating points are colored.

as Fe^{III},[34] Ga^{III},[35] or others (Fig. 1).[36–38] The oxygen in this sequence can often bind another central metal or lanthanide ion. The most plentiful examples of metallacrowns are the 9-MC-3, the 12-MC-4, and the 15-MC-5 motifs. In the general notation n_1-MC-n_2, n_1 represents the number of atoms in the ring, while n_2 represents the number of those atoms which are a metal ion. Because of the tendency to form common structures, many complexes can be created with an isostructural ligand set, but a diverse metal composition. Additionally, provided that a similar bonding motif is maintained in the ligand set, a diversity of ligands can be used to form isometallic compounds.[31,39–43]

For optimal MCE performance (*vide infra*), an isotropic large spin ground state (S) with large spin degeneracy ($2S + 1$) and hence large magnetic entropy is required. In addition, improved performance can be obtained if the excited spin states are close to the ground one increasing the spin degeneracy. Because the geometry of metallacrowns generally leads to antiferromagnetic coupling (J_1) between metal ions within the ring (M_2 in Fig. 2), a large ground spin state can only be obtained if the central metal ion (M_1 in Fig. 2) has a large antiferromagnetic exchange coupling (J_2) with the ring ions (M_2) polarizing their spin in the same direction.[33] This is possible because the ring ions are bridged by two atoms (N–O), while the central ion has a single atom bridge (O) with the ring ones (Fig. 1). To ensure a maximum of spin degeneracy, ions with isotropic spin states (Such as $3d^5$ Fe^{III} or $4f^7$ Gd^{III}) are preferred. Finally, metal ions with as large as possible spin values should be used for the ring ions, M_2.

Herein, we present two Gd^{III}[12-$MC_{Fe^{III}(N)(shi)}$-4] metallacrown complexes (Fig. 1) analyzed for the MCE in the temperature region 2–20 K. The complexes are PyH[$Fe_4Gd(shi)_4(PhCO_2)_4$-$(Py)_4$]·(MeOH) (**1**) and [$Fe_4Gd(shi)_4(H_2shi)_3(Py)_3(H_2O)$]·(Py) (**2**), where H_3shi = salicylhydroxamic acid. They each consist of an [–Fe–N–O–]$_4$ metallacrown ring which binds a centrally located Gd^{III} ion. However, the complexes differ in the geometry of their metallacrown rings and in additional bonding modes between certain Gd–Fe pairs.

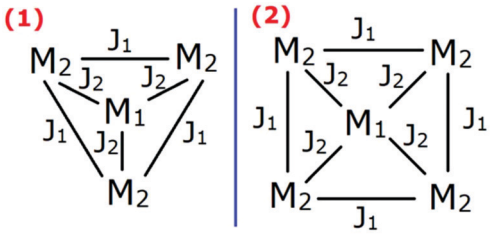

Fig. 2 A magnetic coupling scheme for a 9-MC-3 metallacrown (left) and a 12-MC-4 metallacrown (right). In this scheme, all the ring metals (M_2) are considered as behaving identically to one another, and all have identical coupling to the central metal ion (J_2 = M_1–O–M_2) and to each adjacent ring metal ion (J_1 = M_2–N–O–M_2).

The second complex (**2**) is more distorted than the first (**1**) allowing for evaluation of the effects of the distortion on the magnitude of the exchange coupling. The first complex (**1**) was described previously,[44] but a full analysis of its magnetic and MCE is given and compared to those of **1**. We also devise a scheme to optimize MCE behavior in 12-MC-4 Fe^{III} based metallacrowns by analyzing the relative magnitudes of the exchange coupling parameters J_1 and J_2 in a series of metallacrown complexes.

Materials and methods

Synthesis

All reagents and chemicals were purchased from commercial sources and used without further purification. All reactions were carried out aerobically under ambient conditions. Elemental analysis was performed by Atlantic Microlabs Inc. ESI-MS spectra were collected with an Agilent 6230 TOF HPLC-MS mass spectrometer in negative ion mode (–350 V) on sample dissolved in methanol. Only **1** was stable to MS.

PyH[$Fe_4Gd(shi)_4(PhCO_2)_4(Py)_4$]·(MeOH) (1)

Synthesized as previously described.[44] Elemental analysis calculated for $GdFe_4C_{82}H_{66}N_9O_{21}$: C, 52.00; H, 3.51; N, 6.66. Found: C, 52.09; H, 3.46; N, 6.88. ESI-MS calculated for [$Fe_4Gd(shi)_4(PhCO_2)_4]^-$, $C_{56}H_{36}N_4O_{20}Fe_4Gd$, 1465.86; found, 1465.85.

[$Fe_4Gd(shi)_4(H_2shi)_3(Py)_3(H_2O)$]·(Py) (2)

Salicylhydroxamic acid (shi, 0.875 mmol, 0.134 g), $Gd(NO_3)_3·6H_2O$ (0.125 mmol, 0.043 g) and $Fe(NO_3)_3·9H_2O$ (0.50 mmol, 0.202 g) were dissolved in 46 mL methanol. To the stirring solution, 6 mL pyridine (Py, 776.6 mmol) was added dropwise, followed by 6.5 mL H_2O. The solution was stirred for

30 seconds then filtered. Vapor diffusion in a water chamber yielded crystals after several days. These were collected *via* filtration and dried in air. Yield: 0.037 g, 16.5% by mass. Elemental analysis calculated for $GdFe_4C_{69}H_{56}N_{11}O_{22}$: C, 46.77; H, 3.19; N, 8.70. Found: C, 47.23; H, 3.24; N, 9.16.

Crystallography

Brown needles of **2** were grown from a methanol/water/pyridine solution of the compound at 22 °C. A crystal of dimensions 0.14 × 0.04 × 0.04 mm was mounted on a Rigaku AFC10K Saturn 944+ CCD-based X-ray diffractometer equipped with a low temperature device and Micromax-007HF Cu-target micro-focus rotating anode (λ = 1.54187 Å) operated at 1.2 kW power (40 kV, 30 mA). The X-ray intensities were measured at 85(1) K with the detector placed at a distance 42.00 mm from the crystal. A total of 2028 images were collected with an oscillation width of 1.0° in ω. The exposure times were 1 s. for the low angle images, 10 s. for high angle. Rigaku d*trek images were exported to CrysAlisPro for processing and corrected for absorption.[45,46] The integration of the data yielded a total of 268 915 reflections to a maximum 2θ value of 139.68° of which 16 817 were independent and 13 731 were greater than $2\sigma(I)$. The final cell constants (Table S1†) were based on the xyz centroids of 38 340 reflections above $10\sigma(I)$. Analysis of the data showed negligible decay during data collection. The structure was solved and refined with the Bruker SHELXTL (version 2018/3) software package,[47] using the space group *Pbca* with Z = 8. All non-hydrogen atoms were refined anisotropically with the hydrogen atoms placed in idealized or refined positions. Full matrix least-squares refinement based on F^2 converged at R_1 = 0.0773 and wR_2 = 0.2082 [based on $I > 2\sigma(I)$], R_1 = 0.0918 and wR_2 = 0.2250 for all data. Additional details are presented in Table S1 and are given as ESI† in a CIF file.

DC magnetometry

Magnetic measurements were performed in a Quantum Design MPMS X L7 SQUID magnetometer. Samples were lightly ground in a mortar and pestle to homogenize, then placed in a gelatin capsule with a small amount of melted eicosane. The eicosane was allowed to solidify to prevent sample torqueing at high fields. Variable temperature DC measurements were performed from 2–300 K with a 0.2 T applied field. Variable field, variable temperature DC measurements were performed from 2–20 K with fields ranging from 0–7 T. Diamagnetic corrections were applied based on Pascal's constants.

Results and discussion

Synthesis

The two compounds were synthesized in a methanol/pyridine solution by stoichiometrically mixing the requisite starting materials ($Fe(NO_3)_3$, $Gd(NO_3)_3$, and H_3shi) in accordance with the composition of the final product. The main difference in the two synthetic procedures is the availability of benzoate to serve as a coordinating ligand for **1**, and otherwise the procedures are quite similar. Accordingly, **1** has a composition $PyH[Fe_4Gd(shi)_4(PhCO_2)_4(Py)_4]\cdot(MeOH)$ while **2** has the composition $[Fe_4Gd(shi)_4(H_2shi)_3(Py)_3(H_2O)]\cdot(Py)$. Complex **2** was synthesized with nitrate salts of Fe^{3+} and Gd^{3+}, nitrate salts being commonly used in the synthesis of many similar metallacrowns[35,44,48–50] A great excess of pyridine ensures that it acts as a base, solvent, and coordinating ligand. While a very short stirring time was used, the stable formation of these macrocycles likely occurs only as the compounds crystallize out of solution. This is consistent with the lack of solution stability suggested by the lack of appearance of the complex in mass spectrometry. Other Ga^{3+}/shi/Ln^{3+} metallacrown cluster compounds used similar synthetic conditions.[51]

Structural considerations

Complex **1** is briefly described here to facilitate an adequate comparison to **2**.[44] Complex **1** ($PyH[Fe_4Gd(shi)_4(PhCO_2)_4(Py)_4]\cdot(MeOH)$, Fig. 3) is anionic and has a pyridinium (PyH) counterion. It is a 12-$MC_{Fe^{III}(N)(shi)}$-4 structure (see Fig. 1 and S1–S4†), however, rather than a flat metallacrown ring, one of the ligands is folded below the plane. The planar position normally containing the shi^{3-} is instead occupied by two pyridine ligands. A Gd^{III} ion fills the central cavity of the complex, bonded in a pseudo square antiprismatic GdO_8 geometry with the four shi^{3-} oxime oxygens forming one plane, and four benzoate oxygens filling the remaining four planar positions (Fig. 3). The Gd^{III} lies in the center of the metallacrown cavity but is displaced above the metallacrown ring plane by 1.713 Å.

Complex **2** ($[Fe_4Gd(shi)_4(H_2shi)_3(Py)_3(H_2O)]\cdot(Py)$, Fig. 3, S3, and S5–S7†) is neutral. In addition to the four tri-deprotonated shi^{3-} ligands in the metallacrown ring, **2**, it has three additional mono-deprotonated H_2shi^- ligands filling the set. Conversely, **1** has four benzoate anions completing the set. All four Fe^{III} are crystallographically inequivalent. Complex **2** is a 12-$MC_{Fe^{III}(N)(shi)}$-4 structure, with a bent geometry where the metallacrown ring presents a butterfly-type topology creasing at two opposite Fe^{III} ions. According to the labeling scheme specified in Fig. 3, Fe-2 and Fe-4 represent the "body" while Fe-1 and Fe-3 represent the "wingtips" of the butterfly shape (Fig. 3).

Within the crystal structure, two distinct isomeric complexes exist, which are related by an inversion center (Fig. S3†). When considering the shi^{3-} ligands as bidentate for each Fe^{III} (either from hydroximate N to phenolic O sequence [N–C–C–C–O]; or hydroximate oxime O to hydroximate carbonyl O [O–N–C–O]): **1** has one complex with one planar Fe^{III} configuration, one Λ propeller configuration, and two Δ propeller configurations. As required, the inversion related counterpart has one planar Fe^{III} configuration, two Λ propeller configurations, and one Δ propeller configuration, where the chiral assignments are opposite of the inversion-related counterpart (Fig. S7†). These local structural constraints are responsible for the non-planar structural orientation of the molecule. They are also interesting in that prior metallacrowns that had mixtures

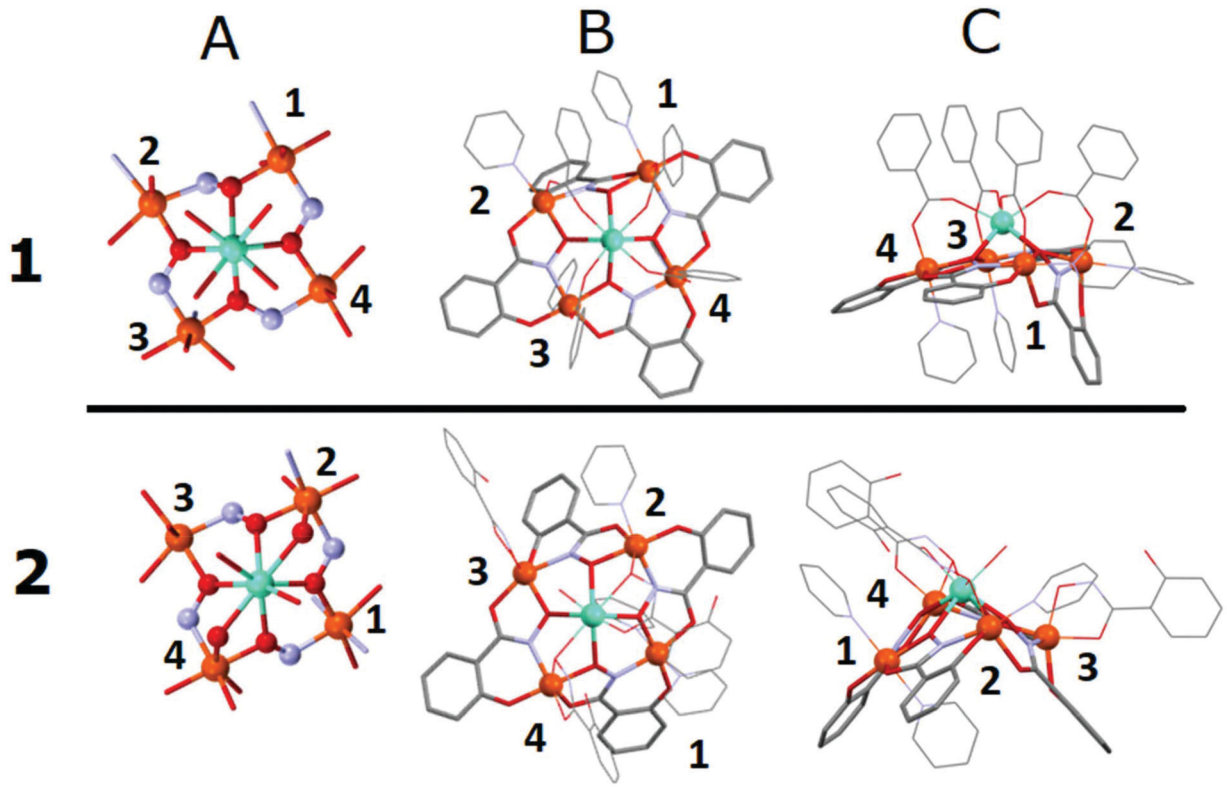

Fig. 3 Multiple views of complexes **1** and **2**. Cross-cavity Fe^{III}–Fe^{III} distances are 6.648 and 6.505 Å for **1**, and 6.710 and 6.387 Å for **2**. Hydrogens and nonbonding solvents of crystallization are omitted in every case for clarity. Common color scheme: Fe, orange; Gd, teal; N, light blue; O, red; C, grey. The Fe^{III} are labeled as described in the text. (A) Top–down view displaying only the metal ions and the primary coordination sphere. Metal ions and coupling intermediary atoms are shown as spheres, other atoms shown as rods. (B) Top–down view emphasizing the metallacrown ring. Metal ions shown as spheres, metallacrown framework shown as rods, and other coordinating ligands shown in wireframe. (C) Side-on view emphasizing geometry of metallacrown ring. Numbering of the Fe atoms corresponds to measurements in Table 1.

of propeller and planar configurations had symmetric numbers of each isomer (*e.g.*, 9-MC-3 contained either 3Λ or 3Δ centers;[33,34] whereas 15-MC-5 required Λ, Δ, Λ with 2 planar centers closing the metallacrown ring;[52] or 18-MC-6 structures that alternated Λ and Δ sites[53]).

Complex **1** is more uniform than **2**, which is more ruffled and possesses an additional Fe–O–Gd interaction between each of the two "butterfly body" Fe^{III} and the central Gd^{III}. A more detailed description of the structures is given in the ESI.†

DC magnetic properties

The $\chi_M T$ values (around 22 cm^3 mol^{-1} K) for **1** and **2** at room temperature are slightly lower than those expected for four non-interacting high spin Fe(III) (S = 5/2) and one Gd(III) (S = 7/2), with a value equal to 25.0 cm^3 mol^{-1} K assuming g_{Fe} = 1.98 and g_{Gd} = 2.00 (Fig. 4). Upon cooling, $\chi_M T$ decreases and reaches 7.6 and 7.2 cm^3 mol^{-1} K for **1** and **2** respectively, indicating an overall antiferromagnetic interaction for the two compounds. The $\chi_M T$ values for the two compounds are very close to those of an isolated S = 7/2 (7.9 cm^3 mol^{-1} K). The magnetization (M) *vs.* the applied magnetic field (B) were measured in the T = 2–20 K range for **1** and **2** (Fig. 5). For T = 2 K, the magnetization curves do not saturate but their values are very close to 7 Bohr Magnetons at B = 7 T. Their shape is very close to the Brillouin function of an S = 7/2 (g = 2)

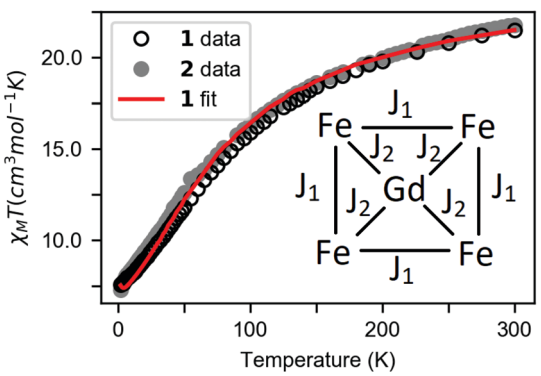

Fig. 4 Magnetic susceptibility data for complexes **1** and **2**, as well as the fit for complex **1**. Powder data collected with a 0.2 T applied magnetic field from 2–300 K. Fit obtained *via* simultaneous fit of the present magnetic susceptibility data and the magnetization data presented in Fig. S9† to eqn (1). The coupling scheme for the fitting is given in the inset: where J_1 represents Fe^{III}–N–O–Fe^{III} bonds and J_2 represents Gd^{III}–O–Fe^{III} bonds.

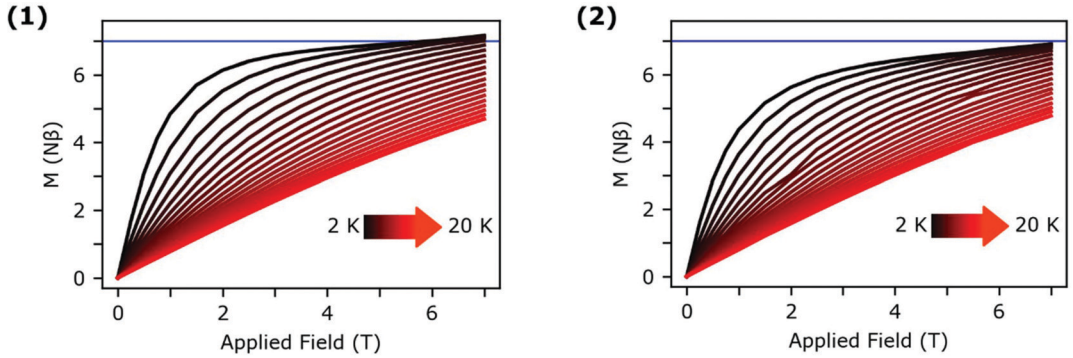

Fig. 5 Temperature dependent magnetization data for **1** (left) and **2** (right). Data presented as Bohr magnetons per molecule ($N\beta$) with a field sweep from 0–7 T. Temperature sweep is from 2–20 K with 1 K step-sizes. The blue line at $7N\beta$ indicates the magnetization of a pure S = 7/2 spin system, such as a free-ion Gd^{III}. The fit of these data for **1** is given in Fig. S9.†

(Fig. S8†). These data are consistent with an overall antiferromagnetic exchange coupling among the metal ions that is larger among the four S = 5/2 Fe(III) ions than between the central S = 7/2 Gd(III) and the four peripheral Fe(III) ions.

To analyze the magnetic behavior of the complexes quantitatively, the magnetic susceptibility and magnetization curves were simultaneously fit using the PHI package.[54] Since high-spin S = 5/2 Fe^{III} and S = 7/2 Gd^{III} ions do not possess first order orbital angular momentum, a quantitative fit is obtained using the spin-only Hamiltonian given below. The magnetic data of **1** fit well to the spin-only Hamiltonian corresponding to the coupling scheme shown in Fig. 4-inset.

$$\hat{H} = -J_1(\hat{S}_2 \cdot \hat{S}_3 + \hat{S}_3 \cdot \hat{S}_4 + \hat{S}_4 \cdot \hat{S}_5 + \hat{S}_2 \cdot \hat{S}_5) - J_2(\hat{S}_1 \cdot \hat{S}_2 + \hat{S}_1 \cdot \hat{S}_3 + \hat{S}_1 \cdot \hat{S}_4 + \hat{S}_1 \cdot \hat{S}_5) + \hat{H}_{ZE} \quad (1a)$$

$$\hat{H}_{ZE} = \beta \sum_{i=1}^{N} \hat{S}_i \cdot g_i \cdot \vec{B} \quad (1b)$$

where J_1, and J_2 are exchange coupling parameters among the ring and between the central and the ring ions, respectively; $\hat{S}_i$ are the spin operators, noting specifically that $\hat{S}_1$ corresponds to the Gd^{III} (central ion) and $\hat{S}_2$–$\hat{S}_5$ to the Fe^{III} (ring metal ion) centers. $\hat{H}_{ZE}$ is the Zeeman Hamiltonian, where β is the Bohr magneton, g_i is the spin-center dependent g-tensor considered isotropic here, and $\vec{B}$ is the applied magnetic field. During the fitting procedure, for Gd^{III}, g was held at 2.00 and for Fe^{III}, g was held at 1.98. This models all exchange interactions as identical between adjacent Fe^{III}–Fe^{III} and each Fe^{III}–Gd^{III} pair (Fig. 4 and S9†). Fe^{III}–Fe^{III} coupling was found as J_1 = −7.46 cm^{-1}, and Fe^{III}–Gd^{III} coupling was found to be J_2 = −0.72 cm^{-1}. The Fe^{III}–Fe^{III} exchange is similar to parameters derived from other Fe^{III}–N–O–Fe^{III} bridged metallacrowns, where values of −6.0 cm^{-1} and *ca.* −9 cm^{-1} were previously obtained.[33,55] The small Gd^{III}–Fe^{III} coupling parameter is consistent with the typically weak nature of 4f element exchange.[51,56]

A similar fitting was attempted for complex **2** keeping one exchange coupling parameter (J_1) among the Fe^{III} ions but using two different parameters (J_2 and J'_2) between Fe^{III} and Gd^{III} (considering J_2 = Fe^{III}–O–Gd^{III} coupling for the two wingtip Fe^{III} and J'_2 = Fe^{III}–O–Gd^{III} coupling for the two butterfly body Fe^{III}). Fair results were obtained with J_1 (Fe^{III}–O–Fe^{III}) ≈ −7 to −9 cm^{-1}, and J_2, J'_2 ≈ −1.0 to +0.2 cm^{-1}. The fit of the $\chi_M T$ data above 6 K is excellent, but discrepancies appear at low temperature that are more visible in the $M = f(B)$ plots (Fig. S10†). It is likely that this complex has a myriad of nonequivalent interactions which preclude a simple fit as obtained for **1** (Fig. 3 and Table 1). Further fitting attempts with a larger number of parameters were not pursued to avoid overparameterization.

By comparing the experimental magnetization curves at 2 K (Fig. S8†), we see that the magnetization curve for **2** is below that of **1**, even though they reach almost the same value (close to 7 Bohr Magnetons) at B = 7 T. This is consistent with either (i) a large number of low-lying spin states very close in energy, among them an S = 7/2 state; or (ii) a spin ground state lower than 7/2 with the S = 7/2 state close in energy for **2**, while for **1** the ground state is S = 7/2 relatively separated from the excited ones. Such behavior is in line with the larger structural differences in the Fe^{III}–Gd^{III} linkages for **2** than for **1** that result in additional coupling exchange parameters for the former than for the latter. However, despite the different shapes of **1** and **2** and the difference in their ring structure (Table 1) the values of the exchange coupling parameters (J_1) are almost the same, probably because they are mainly controlled by the –Fe^{III}–N–O–Fe^{III}-linkage. This is also the case for other Fe^{III} containing metallacrowns,[33,55] Therefore, changes in the structural parameters hardly influence the magnitude of the in-ring magnetic coupling for the 12-$MC_{Fe^{III}(N-O)}$-4 metallacrowns. This property of metallacrown complexes will be exploited to propose a strategy for enhancing MCE.

Magnetocaloric effect

The magnetocaloric effect can be described as the change in temperature of a material with a changing magnetic field. One way to quantify this effect comes from the funda-

Table 1 Structural comparison of the metallacrown ring's $-[Fe-N-O]_n$-bonds, and of the Fe–O–Gd bonds for **1** and **2**

	1				**2**			
Fe–N–O–Fe component	Fe–N–O–Fe torsion (°)	Fe–N distance (Å)	N–O distance (Å)	O–Fe distance (Å)	Fe–N–O–Fe torsion (°)	Fe–N distance (Å)	N–O distance (Å)	O–Fe distance (Å)
1	153.53	2.012	1.402	1.948	178.08	2.053	1.403	1.990
2	173.64	2.055	1.386	2.005	168.77	2.064	1.403	2.010
3	169.42	2.034	1.413	1.974	170.01	2.018	1.404	2.020
4	171.15	2.053	1.375	2.011	172.64	2.049	1.408	2.030
Fe–O–Gd component	Fe–O–Gd angle (°)	Fe–O distance (Å)	O–Gd distance (Å)		Fe–O–Gd angle[a] (°)	Fe–O distance[a] (Å)	O–Gd distance[a] (Å)	
1	123.21	1.948	2.320		130.01	2.010	2.380	
2	118.75	2.005	2.341		108.42	1.990	2.298	
					99.52	2.065	2.484	
3	119.30	1.974	2.398		122.88	2.030	2.384	
4	118.07	2.011	2.432		106.24	2.020	2.350	
					99.49	2.091	2.485	

[a] Six bonds are reported (rather than four) since two of the Fe–Gd units have two Fe–O–Gd bonds.

mental Maxwell relation (eqn (2a)) and its transformation (eqn (2b)):

$$\left(\frac{\partial S_m}{\partial B}\right)_T = \left(\frac{\partial M}{\partial T}\right)_B \quad (2a)$$

$$\Delta S_m = \int_0^B \left(\frac{\partial M(T,B)}{\partial T}\right)_B dB \quad (2b)$$

ΔS_m is the isothermal magnetic entropy change, which serves as an experimentally available measure for analyzing the performance of a magnetocaloric material. Eqn (2b) represents an experimental prescription for finding ΔS_m. Variable field (B), variable temperature (T) magnetization (M) experimental results are given in Fig. 5. These data can be quantitatively analyzed *via* eqn (2b) to determine ΔS_m.

Fig. 6 presents the temperature dependent magnetic entropy change for **1** and **2** in the 3–20 K range. The data are given (as is common) in the negative ΔS_m sense to yield a positive representation. To build a better magnetocaloric agent material, a large value of $-\Delta S_m$ is desired such that changes in the applied field can lead to large changes in magnetization, and hence large changes in temperature. To facilitate comparison between materials, such $-\Delta S_m$ plots are typically presented in the per mass basis, as given in Fig. 6 (the molar basis is given in Fig. S11†). Here, for both **1** and **2** there is an increase in $-\Delta S_m$ toward lower temperatures, with complex **2** peaking *ca.* 4 K with a 7 T field sweep, and complex **1** appearing to almost peak around 3 K. Such behavior is typical of weakly coupled molecular magnetic materials.[10] Complex **1** has an experimental maximum of 7.3 J K^{-1} kg^{-1} at 3 K, and **2** peaks at 6.1 J K^{-1} kg^{-1} at 4 K. At the very low temperature region, the $-\Delta S_m$ behavior is similar between 5 T and 7 T field sweeps, suggesting only a weak $-\Delta S_m$ material property gain with the higher field sweep. The MCE properties of **1** and **2** are weak compared to other molecular materials. For example, many Fe^{III} based materials have low-temperature $-\Delta S_m$ in excess of 15 J K^{-1} kg^{-1},[15–18,33] and multiple 3d–4f materials have $-\Delta S_m$ over 30 J K^{-1} kg^{-1} with a 7 T field sweep.[21,25,27,57–60] This can be understood owing to the small density of low-lying magnetic states for the present materials as observed in Fig. 7 and Fig. S12.†

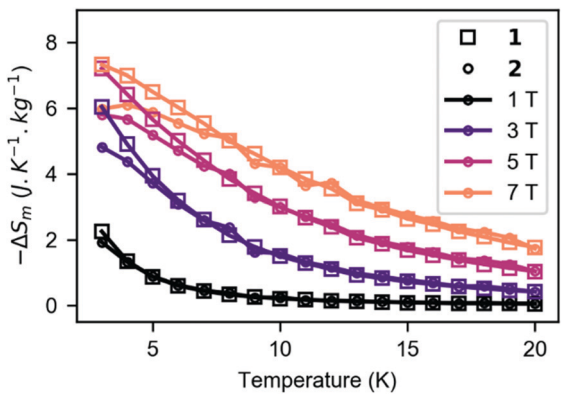

Fig. 6 Temperature dependent magnetic entropy change (per kg material) in the range 3–20 K. Plot obtained from a numerical evaluation of the data in Fig. 5 according to eqn (2b) with integration from 0 to 1, 3, 5, and 7 Tesla. Complex **1** data shown as squares, complex **2** as circles. At B = 7 T, the maximum for **1** is 7.3 J K^{-1} kg^{-1} at 3 K, and for **2** is 6.1 J K^{-1} kg^{-1} at 4 K. The molar basis presented in Fig. S11.†

If the energy levels and their degeneracy can be calculated (*e.g.* from a spin Hamiltonian), the $S_m^{zerofield}$ can be calculated (S_m^{Calc}, see ESI, particularly eqn (S1)–(S3)†). The upper limit of $-\Delta S_m$ can be estimated by assuming that only one state is occupied during magnetization, since $\Delta S_m \approx S_m^{appliedfield} - S_m^{zerofield}$. This yields the upper limit $-\Delta S_m^{Calc}$ (upper limit) = $S_m^{zerofield}$ (S_m^{Calc}) if $S_m^{appliedfield}$ = 0 as when only one state is occupied during magnetization (in practice it will likely be less as the moment will not usually be fully saturated into one single state). Higher entropy at zero field should correspond then to a higher upper limit for $-\Delta S_m$.

It is instructive to observe the S_m properties of each system in the molar basis to facilitate a more direct comparison.

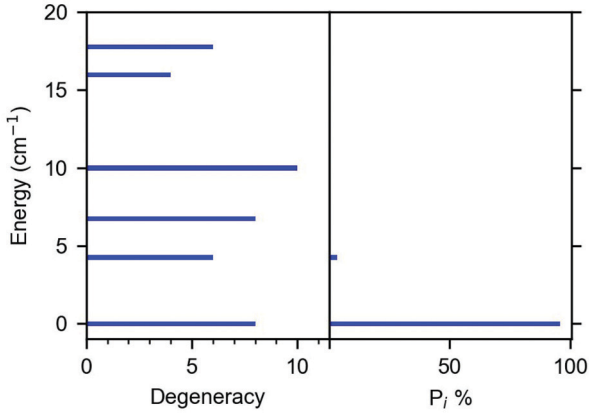

Fig. 7 Spin state energy levels determined *via* fitting the spin Hamiltonian to the data for **1** by the PHI package. (Left) This figure plots the energy of each spin state as well as the level's degeneracy in zero applied magnetic fields. Energy levels from 0–20 cm^{-1}, and the population (right) of each level determined *via* the Boltzmann distribution. The ground degeneracy of 8 suggests an S = 7/2 ground spin state (2 × (7/2) + 1 = 8). The population for each state is calculated at 2 K, 95.8% ground, 4.2% first excited state at 2 K.

Using the energy levels for **1** calculated by Kambe's method, S_m^{Calc} for **1** was calculated as 17.65 J K^{-1} mol^{-1} at 2 K (18.43 J K^{-1} mol^{-1} at 3 K). These are slightly above the calculated ground state value of 17.29 J K^{-1} mol^{-1} when only the ground state (S = 7/2) is considered. This is because the S = 5/2 state lying 4.25 cm^{-1} above the ground state is also slightly thermally populated (Fig. 7), therefore, it is contributing to the magnetic entropy. However, the measured molar $-\Delta S_m$ value (13.87 J K^{-1} mol^{-1} with 7 T sweep Fig. S11†) is in fact lower than the S_m^{Calc} value, probably because the magnetic moment is not fully saturated into a single state during the magnetization phase, so $S_m^{appliedfield} \neq 0$.

Complex **2** has a slightly larger difference $J(Fe^{III}–Fe^{III}) – J(Fe^{III}–Gd^{III})$ than **1**. This is due to a combination of different $Fe^{III}–Fe^{III}$ couplings and/or increased $Fe^{III}–Gd^{III}$ couplings. This will result in a lower density of spin states at low energy for **2** than **1** and a reduction in MCE performance. The antiferromagnetic coupling in these compounds means that the four non-contributing ions (the ring Fe^{III}) are essentially "dead weight" since the are minimally contributing at low temperatures. The non-contributing mass of the Fe^{III} and the templating ligands combine to decrease the MCE (per mass) performance of this system.

For an effective MCE material, a high density of low-lying magnetic states should be available such that they can be accessed thermally once the applied magnetic field is removed. This is attainable by changing the J_2/J_1 ratio assuming antiferromagnetic exchange couplings as is the case for metallacrown complexes.

Using the Hamiltonian parameters for each complex, and the corresponding energy levels for each system as calculated from either Kambe's method[61] or the Phi package,[54] we computed the energies of the magnetic states and the corresponding entropy (see "Calculating the magnetic entropy at 2 K" in the ESI,† S_m^{Calc} at T = 2 K and B = 0 T) for $GdFe_4$ as a function of J_1/J_2 (Fig. 8). It is found that the largest entropy occurs where nodes exist such that different spin states are degenerate. For example, at J_1/J_2 = 0.35 the S = 13/2 and 11/2 states are degenerate. When both J_1 and J_2 are very small, many states become simultaneously thermally occupiable at 2 K and the entropy increases accordingly. For any J_2 value, S_m^{Calc} remains relatively large when J_1/J_2 is smaller than 0.35 where the ground spin state is equal to 13/2. This corresponds to the situation where the ring spins are all parallel. Unfortunately, such a situation is not attainable for $GdFe_4$ because it requires a large antiferromagnetic coupling ($|J_2|$ > 20 cm^{-1} assuming J_1 = −7 cm^{-1}) between Gd^{III} and Fe^{III} which is not possible because of the weak delocalization of the f elec-

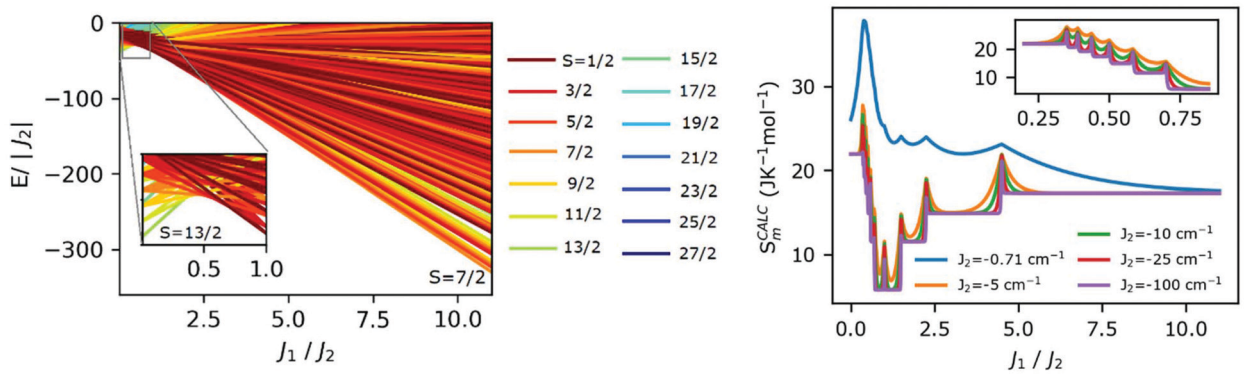

Fig. 8 (Left) Lower portion of the energy diagram for the spin states of $Gd^{III}Fe^{III}_4$ plotted as $E/|J_2|$ *vs.* J_1/J_2.[62] For an S = 13/2 ground state, a J_1/J_2 ratio < *ca.* 0.35 is necessary. The experimental ratio J_1/J_2 is 10.6, indicating an S = 7/2 ground state. (Right) Entropy of a $GdFe_4$ system at 2 K without an applied field as a function of the J_1/J_2 ratio for several different values of J_2. The inset shows the values from J_1/J_2 = *ca.* 0.2 to 0.8 for several J_2 values for emphasis. The peaks are nodes where different spin states are degenerate, which increases the ground state degeneracy and thus the entropy. Each peak broadens with smaller J_2 as this increases the number of states which can be thermally occupied at 2 K. Complex **1** has J_1/J_2 = 10.6 with J_2 = −0.71, corresponding to S_m^{Calc} = 17.65 J K^{-1} mol^{-1}.

trons. Since one cannot significantly adjust the Gd^{3+}–Fe^{3+} coupling in the present system due to the inherently very weak nature of lanthanide ion exchange, unlocking the higher entropy states for the $GdFe_4$ complex is likely impossible. However, exchanging the central lanthanide for a transition metal ion (M′) with more delocalized d electrons should lead to larger central-ring antiferromagnetic exchange coupling that may stabilize a larger ground spin state for a similar $M'Fe_4$ compound. So, in the present case, despite the large amount of spin available on the $GdFe_4$ complexes, the greatest density of magnetic states lies at higher energies. These higher energy states are not congruent with thermal occupation in the temperature range where magnetization occurs most effectively for this system (at very low temperatures), so these higher energy spin states cannot be accessed and are generally non-contributing to the MCE.

While these metallacrowns do not necessarily represent advanced MCE materials in the absolute sense, it is quite instructive to compare the magnetic properties between isostructural metallacrown materials having different ring and centrally bound metal ions. This can be done in a theoretical sense by using previously (experimentally) determined exchange coupling parameters for several metallacrown complexes (Table 2).

We now compare the present Gd^{III}[12-$MC_{Fe^{III}N(shi)}$-4] materials to two previous Fe^{III}[9-$MC_{Fe^{III}N(shi)}$-3] complexes which were analyzed for the magnetocaloric effect.[33] These previous complexes consisted of a 9-MC-3 metallacrown with three crystallographically equivalent Fe^{III} in the ring and one Fe^{III} in the central cavity, where the central and outer Fe^{III} are additionally bridged by either an acetate or benzoate-derived carboxylate group (as in Fe^{III}–O–C–O–Fe^{III}). This is contrasted by **1** and **2** which are 12-MC-4 metallacrowns with four Fe^{III} in the ring and a Gd^{III} bound in the central cavity. The Fe^{III}[9-$MC_{Fe^{III}N(shi)}$-3] complexes had antiferromagnetic ring J_1 (Fe^{III}–Fe^{III} exchange) values of −4.5 and −6.4 cm^{-1} for the benzoate and acetate bridged complexes, respectively. Cavity Fe^{III}-ring Fe^{III} J_2 values of −24.9 and −28.0 cm^{-1} for the benzoate and acetate bridged complexes were determined, respectively. The J_1 values are comparable to those determined for **1** (J_1 = −7.5), but the antiferromagnetic central metal-ring metal coupling is much stronger for the 9-MC-3s than **1** ($|J_2|$ > 20 *vs.* 0.71 cm^{-1}, respectively), to be expected in 3d–3d *vs.* 3d–4f coupling. These Fe^{III}[9-$MC_{Fe^{III}N(shi)}$-3] complexes had better MCE performance ($-\Delta S_m$ = 7.4 and 15.4 J kg^{-1} K^{-1} for benzoate and acetate, respectively at 3 K with a 7 T field sweep) than the present Gd^{III}[12-$MC_{Fe^{III}N(shi)}$-4] materials (7.3 and 6.1 J kg^{-1} K^{-1} for **1** and **2** at 3 K with a 7 T field sweep, respectively) despite having a smaller amount of spin available (four Fe^{III} *vs.* four Fe^{III} and one Gd^{III}), and a stronger antiferromagnetic J_2 coupling. This can be rationalized principally by the larger spin ground state of $FeFe_3$ than of $GdFe_4$ because of the larger central-ring (J_2) antiferromagnetic coupling.

Using the Hamiltonian parameters for each complex Fe^{III}[9-$MC_{Fe^{III}N(shi)}$-3]-1 and Fe^{III}[9-$MC_{Fe^{III}N(shi)}$-3]-2, and the corresponding energy levels for each system as calculated from either Kambe's method[61] or the Phi package,[54] S_m^{Calc} was calculated from eqn (S1) and (S2).† For Fe^{III}[9-$MC_{Fe^{III}N(shi)}$-3]-1, S_m^{Calc} was calculated to be 19.94 J K^{-1} mol^{-1} (Fig. S13†). This is larger than the maximum experimental value ∼9.2 J K^{-1} mol^{-1} at 7 K, understandable due to the relatively large intermolecular antiferromagnetic coupling for this complex (zJ = −0.69 cm^{-1}) which reduces spin density at low temperatures.

The comparison for Fe^{III}[9-$MC_{Fe^{III}N(shi)}$-3]-2 is even more insightful. In the original publication, a zero-field splitting (ZFS) axial parameter (D) was included in the Hamiltonian fitting the data for Fe^{III}[9-$MC_{Fe^{III}N(shi)}$-3]-2 to account for low-temperature $\chi_M T$ behavior, however, antiferromagnetic intermolecular interactions can also produce a similar accounting for such behavior. By comparing the calculated energy level diagram, the calculated magnetic entropy S_m^{Calc}, and the experimental $-\Delta S_m$ value, one can potentially distinguish between low temperature phenomena such as intermolecular interactions (zJ) or ZFS. The energy level diagram and S_m^{Calc} were calculated using each the D = −0.3 cm^{-1} or zJ = −0.001 cm^{-1}. Both produce similar calculated $\chi_M T$ curves (Fig. S14†), but yield notably different S_m^{Calc} values: 8.79 J K^{-1} mol^{-1} when ZFS is considered (Fig. S15†) *vs.* 19.94 when zJ is considered (Fig. S16†) at 2 K. The difference comes from the splitting of the energy levels in the ZFS scheme, which splits the 11-fold degenerate (S = 10/2) state into 6 different states. Only the new 2-fold degenerate ground state has a population greater than 25%, the rest have minimal thermal occupation. For the zJ scheme, with 11-fold ground degeneracy, S_m^{Calc} is much greater. When comparing to the experimental results: $-\Delta S_m$ = 16.8 J K^{-1} mol^{-1} at 3 K, it is apparent that the ZFS description is

Table 2 A collection of structural and magnetic parameters relating to metallacrown complexes

No.	Metallacrown	J_1 (cm^{-1})	J_2 (cm^{-1})	S_{ground}	$-Nk_B \ln(2S_{ground}+1)$ (J K^{-1} mol^{-1})	S_m^{Calc} (J K^{-1} mol^{-1})	Ref.
1	Gd^{III}[12-$MC_{Fe^{III}N(shi)}$-4]	−7.5	−0.71	7/2	17.29	17.65	This work
3	Fe^{III}[9-$MC_{Fe^{III}N(shi)}$-3]-1	−4.5	−24.9	5	19.94	19.94	33
4	Fe^{III}[9-$MC_{Fe^{III}N(shi)}$-3]-2	−6.4	−28.0	5	19.94	19.94	33
5	Cu^{II}[12-$MC_{Fe^{III}N(shi)}$-4]	−7.6	−98.4	11/2	20.66	21.66	31

All complexes were fitted to a 2-J component spin-only Hamiltonian. S_{ground} is the spin present in the energy diagram dictated by the J_1 and J_2 parameters. All exchange parameters were corrected to the notation given in eqn (1), such that J_1 refers to nearest-neighbor ring coupling (M_2^{n+}–N–O–M_2^{n+}) and J_2 refers to ring metal-central ion coupling (M_1^{n+}–O–M_2^{n+}). $-Nk_B \ln(2S_{ground}+1)$ is the maximum entropy if only the ground state spin is considered. S_m^{Calc} is calculated from eqn (S1) and (S2)† at 2 K, and the calculated spin energy levels for each complex as described in the text. The metallacrown notation mirrors that given in Fig. 1.

not adequate and that the *zJ* scheme is a better representation, since S_m^{Calc} (ZFS) < $-\Delta S_m^{Experimental}$ < S_m^{Calc} (*zJ*) and the calculated values are upper limits for $-\Delta S_m$. This demonstrates how the magnetic entropy can be used to distinguish between some types of low-temperature magnetic phenomena and confirm the statement that magnetically isotropic metal ions must be used when MCE performance is sought.

We consider now another Fe^{III} metallacrown (Cu^{II}[12-$MC_{Fe^{III}N(shi)}$-4]).[31] Using the Hamiltonian parameters reported by the authors to simulate the energy levels, we find S_m^{Calc} = 21.66 J K^{-1} mol^{-1} (Fig. S17†). This is slightly above the ground-spin (*S* = 11/2) only value of 20.66 J K^{-1} mol^{-1} owing to the thermal population of the two low-lying high-degeneracy excited states ($degeneracy_{excited\ state\ 1}$ = 10 at 3.6 cm^{-1}, $degeneracy_{excited\ state\ 2}$ = 14 at 4.0 cm^{-1}). The molar S_m^{Calc} value is also much larger here than that of the Gd^{III}[12-$MC_{Fe^{III}N(shi)}$-4] complex because J_2 is larger allowing the stabilization of a large spin ground state.

For a high spin $Cu^{II}Fe^{III}_4$ complex, the corresponding energy diagram as a function of J_1/J_2 is given in Fig. S18.† In this instance, J_1/J_2 < 0.05 is necessary to stabilize the *S* = 19/2 (4 × (5/2) − 1/2) spin state. However, the experimentally determined J_1/J_2 ratio is 0.077 (ground spin state equal to 11/2), which is ∼65% larger than the required ratio to stabilize the *S* = 19/2 state. Such a shift is likely difficult to be accessible synthetically, but some clues to do so with other central ions are given below.

One can propose compounds based on an understanding of the optimal J_1/J_2 ratio for a given spin magnitude. For a hypothetical XFe^{III}_4 compound, where X is a transition metal ion with a given spin value, when S_X = 1, 3/2, 2, or 5/2 (such as Ni^{II}, Co^{II}, Mn^{III}, or $Fe^{III}(Mn^{II})$), the corresponding maximum ratios J_1/J_2 to induce maximal ground spin are respectively, 0.099, 0.147, 0.195, or 0.25 (Fig. S18–S22†). Since experimentally determined J_1 values for Fe^{III}–N–O–Fe^{III} are *ca.* −7.5 cm^{-1}, the minimum magnitude necessary J_2 value can be approximated. This value is J_2 = −75 cm^{-1} for Ni^{II}, −51 cm^{-1} for Co^{II}, −38.5 cm^{-1} for Mn^{III}, and −30.0 cm^{-1} for Fe^{III} (Mn^{II}). The maximal ground spins possible for each are S_{ground} = 9 for $Ni^{II}Fe^{III}_4$, S_{ground} = 17/2 for $Co^{II}Fe^{III}_4$, S_{ground} = 8 for $Mn^{III}Fe^{III}_4$, or S_{ground} = 15/2 for $Fe^{III}Fe^{III}_4$ ($Mn^{II}Fe^{III}_4$).

With this understanding, the hypothetical metallacrown complexes would have MCE potential with the trend $Ni^{II}Fe^{III}_4$ > $Co^{II}Fe^{III}_4$ > $Mn^{III}Fe^{III}_4$ > $Fe^{III}Fe^{III}_4$ ($Mn^{II}Fe^{III}_4$) to match the decreasing ground spin of each. Hence for certain cluster arrangements such as the 12MC4, smaller spin value for the central metal ion could lead to a higher ground spin state and better MCE; and larger antiferromagnetic coupling (for J_2 relative to J_1) can make this possible. This is opposed to general heuristics suggesting maximal spin and minimal antiferromagnetic coupling lead to optimal behavior (within this class of compounds at least).

The ability to form such a ground spin state depends on the magnitude of J_2 being above the determined threshold for a maximum possible ground state. An Fe^{III}–O–M^{II} complex (where the bridge is a μ_2-hydroxido from a phenyl ring, and M^{II} is either Mn^{II}, Ni^{II}, or Co^{II}) was identified.[63] Possessing an (isostructural) complex for each compound, and an Fe^{III}–O–M^{II} angle *ca.* 116–118° in each case, the antiferromagnetic coupling between each was −10.8 cm^{-1} for the Co^{II} complex, −19.2 cm^{-1} for the Mn^{II} complex, and −22.4 cm^{-1} for Ni^{II}. The angle is similar to the *ca.* 118–123° for the present $GdFe_4$ complex (**1**) or the angle *ca.* 124° for the $CuFe_4$ complex. For each complex, the coupling is at least 30% different from the required value for the maximal spin state, so the optimum coupling parameters may not be attainable for these metal combinations, but may yet be possible for $Fe^{III}Fe^{III}_3$ as proposed below.

The $Fe^{III}Fe^{III}_3$ structures previously described have J_2 coupling values of −24.9 and −28.0 cm^{-1}. This is quite close to the −30.6 cm^{-1} necessary for an *S* = 15/2 ground state, suggesting that a $Fe^{III}Fe^{III}_4$ complex would possess a maximal ground state provided the J_2 is slightly stronger. Such a compound has not been reported to date, probably because using carboxylate terminal ligands imposes an eight coordination sphere on the central metal ion adapted to lanthanide ions such as Gd^{III} and not to Fe^{III} that is stable in an hexacoordinate octahedral environment.

Happ & Rentschler demonstrated recently that 12-MC-4 metallacrown structure formation with a central 3d metal ion is possible ($Cu^{II}Fe^{III}_4$),[31] providing no bridging ligands outside the plane of the metallacrown are present so that the central metal lies within the plane of the metallacrown ring, accommodating an octahedral coordination sphere for the central ion. Therefore, the isostructural $Fe^{III}Fe^{III}_4$ complex is likely feasible where the Fe^{III} can fit within the plane and have its preferred octahedral arrangement with axial monodentate ligands. Fig. 9 shows the entropy at 2 K for such a system as a function of J_1/J_2 for several values of J_2. Such a complex would have maximal entropy at J_1/J_2 = 0.25 where the *S* = 15/2 and 13/2 states are degenerate, but would have high entropy arising from a ground *S* = 15/2 state provided that J_1/J_2 < 0.25. Assuming $J_1 \approx -7.5$ cm^{-1} for a 12-$MC_{Fe^{III}}$-4 metalla-

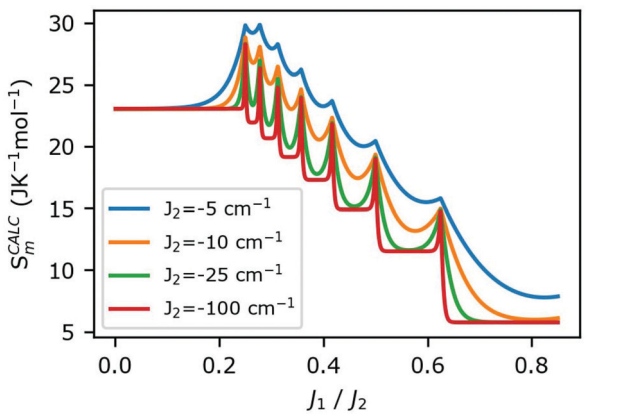

Fig. 9 (Right) Entropy of a hypothetical $Fe^{III}Fe^{III}_4$ system at 2 K without an applied field as a function of the J_1/J_2 ratio for several different values of J_2.

crown (Table 2), J_2 must be $\geq$30 cm^{-1}, although values slightly higher than this can still lead to high ground state degeneracy as the S = 13/2, S = 11/2 degeneracy node is nearby.

Based on the literature reported results, the optimum range of J_1/J_2 to stabilize the large spin state is attainable provided a tuning of the exchange coupling parameters: weak J_1 and large J_2 values are required. Generally, the exchange coupling parameters between metal ions can be tuned not only by the nature of the bridging and related structural parameters, but also by the nature of the peripheral ligands that influence the electronic density of the metal ions. Everything else being equal, decreasing the electronegativity of the peripheral ligands increases the overlap of their p orbitals with the singly occupied magnetic orbitals of the metal ion leading to an increase of the antiferromagnetic exchange coupling parameter.[64] Such effect has been shown to increase the antiferromagnetic coupling in dinuclear Ni(II) and Cu(II) complexes by 50% and 100% respectively.[64,65] Such effect can be used in 12-MC-4 complexes to tune J_1/J_2. For $CuFe_4$, the electron density (related to electronegativity) of the oxygen atom of the salycilylhydroxamate peripheral ligand should be tunable by placing withdrawing or donating groups in the para position (see Fig. 1), leading to a decrease or increase of the coupling between the ring Fe^{III} and central Cu^{II} metal ions. The same effect can be used for $Fe^{III}Fe^{III}{}_4$. For this latter case, axial ligands with large electron donating density on the central Fe^{III} metal ion can increase the antiferromagnetic coupling (J_2) with the ring metal ions, therefore decreasing J_1/J_2 and stabilizing the S = 15/2 ground spin with large entropy change. Finally, considering Fig. 8 and 9 (entropy *vs.* J_1/J_2) one can see that for some ratios of the exchange parameters corresponding to degenerate spin ground states, the entropy in these nodes can be large. However, reaching these particular values is more difficult than just increasing J_2 to stabilize the ferrimagnetic high spin ground state.

This ferrimagnetic strategy, where a central ion is used to polarize each of the surrounding metal ion spins, is not new and was applied successfully to design molecules with high spin ground states in a rational way. For example, the $Cr^{III}(-CN-Mn^{II}L)_6$ complex made from magnetically isotropic metal ions has a spin ground state (S = 27/2) with a large magnetic degeneracy due to the antiferromagnetic coupling between the central and the six peripheral metal ions.[66] The examination of its MCE performance expected to be very high is underway.

Conclusions

Two Gd^{III}[12-$MC_{Fe^{III}(N)(shi)}$-4] metallacrowns were analyzed for magnetic and magnetocaloric properties. Complex **2**, [$Fe_4Gd(shi)_4(H_2shi)_3(Py)_3(H_2O)$], was newly presented. Each of these complexes exhibited similar magnetic properties consistent with Fe–N–O–Fe antiferromagnetic coupling *ca.* J_1 = −7 cm^{-1}, and weaker antiferromagnetic coupling between the centrally bound Gd^{III} and peripheral Fe^{III} ions, *ca.* J_2 = −0.7 cm^{-1}. The slightly different bonding patterns between the complexes did not play a hugely significant role in their magnetic properties as observed in the similarity between magnetization and magnetic susceptibility curves, however, **2** apparently had slightly stronger Fe^{III}–Gd^{III} antiferromagnetic coupling (relative to Fe^{III}–Fe^{III} coupling) consistent with additional bonding modes *versus* **1**.

Based on the study of the magnetic and entropy properties of the two $Gd^{III}Fe^{III}{}_4$ metallacrown complexes here presented and examining data from similar complexes from the literature, we conclude that for the metallacrown family a large central-peripheral antiferromagnetic coupling is required to stabilize a high spin ground state and, therefore, a good MCE performance. To do so, we propose a chemical route for the preparation of a $Fe^{III}Fe^{III}{}_4$ complex, not reported yet, that should have all the requirements for improved MCE performance.

Conflicts of interest

There are no conflicts to declare.

Acknowledgements

This research was supported by the National Science Foundation (NSF) under the grants CHE-1664964 (V. L. P.) and CHE-0840456 for X-ray instrumentation. E. V. S. thanks the Rackham Graduate School for international travel funding as well as NSF grant DGE-1256260.

References

1 R. L. Comstock, Modern magnetic materials in data storage, *J. Mater. Sci.: Mater. Electron.*, 2002, **13**, 509–523.
2 M. Colloms and P. Darlington, *High Performance Loudspeakers*, Wiley, 7th edn, 2018.
3 M. Cheng and Y. Zhu, The state of the art of wind energy conversion systems and technologies: A review, *Energy Convers. Manage.*, 2014, **88**, 332–347.
4 M. Zhu, L. Xia and F. Liu, Unconventional gradient coil designs in magnetic resonance imaging, *Crit. Rev. Biomed. Eng.*, 2014, **42**, 493–526.
5 J. M. D. Coey, *Magnetism and Magnetic Materials*, Cambridge University Press, 2001.
6 P. Wikus, E. Canavan and S. Trowbridge, *Magnetocaloric Materials and the Optimization of Cooling Power Density*, 2018.
7 J. Romero Gómez, R. Ferreiro Garcia, A. De Miguel Catoira and M. Romero Gómez, Magnetocaloric effect: A review of the thermodynamic cycles in magnetic refrigeration, *Renewable Sustainable Energy Rev.*, 2013, **17**, 74–82.
8 H. Zeng, C. Kuang, J. Zhang and M. Yue, Magnetocaloric effect in bulk nanocrystalline Gd metals by spark plasma sintering, *Nanosci. Methods*, 2012, **1**, 16–24.

9 M. Evangelisti, Molecule-Based Magnetic Coolers: Measurement, Design and Application, in *Molecular Magnets, NanoScience and Technology*, ed. J. Bartolomé, F. Luis and J. Fernández, 2014, Springer, Berlin, Heidelberg.
10 J. Liu, Y. Chen, F. Guo and M. Tong, Recent advances in the design of magnetic molecules for use as cryogenic magnetic coolants, *Coord. Chem. Rev.*, 2014, **281**, 26–49.
11 Y.-C. Chen, J. Prokleška, W.-J. Xu, J.-L. Liu, J. Liu, W.-X. Zhang, J. Jia, V. Sechovský and M. Tong, A brilliant cryogenic magnetic coolant: magnetic and magnetocaloric study of ferromagnetically coupled GdF 3, *J. Mater. Chem. C*, 2015, **3**, 12206–12211.
12 L. Ungur, in *Lanthanide-Based Multifunctional Materials: From OLEDs to SIMs*, Elsevier Inc., 2018, pp. 1–58.
13 J. Ferrando-soria, J. Vallejo, M. Castellano, J. Martínez-lillo, E. Pardo, J. Cano, I. Castro, F. Lloret, R. Ruiz-garcía and M. Julve, Molecular magnetism, quo vadis? A historical perspective from a coordination chemist viewpoint, *Coord. Chem. Rev.*, 2017, **339**, 17–103.
14 O. Kahn, *Molecular Magnetism*, VCH Publishers, New York, NY, 1993.
15 M. Evangelisti, A. Candini, A. Ghirri, M. Affronte, S. Piligkos, E. K. Brechin and E. J. L. McInnes, Molecular nanoclusters as magnetic refrigerants: The case of Fe 14 with very large spin ground-state, *Polyhedron*, 2005, **24**, 2573–2578.
16 A. Adhikary, H. S. Jena and S. Konar, A family of Fe^{3+} based double-stranded helicates showing a magnetocaloric effect, and Rhodamine B dye and DNA binding activities, *Dalton Trans.*, 2015, **44**, 15531–15543.
17 R. Shaw, R. H. Laye, L. F. Jones, D. M. Low, C. Talbot-Eeckelaers, Q. Wei, C. J. Milios, S. Teat, M. Helliwell, J. Raftery, M. Evangelisti, M. Affronte, D. Collison, E. K. Brechin and E. J. L. McInnes, 1,2,3-Triazolate-bridged tetradecametallic transition metal clusters [M14(L)6O6(OMe)18X6] (M = Fe^{III}, Cr^{III} and V^{III}/IV) and related compounds: Ground-state spins ranging from S = 0 to S = 25 and spin-enhanced magnetocaloric effect, *Inorg. Chem.*, 2007, **46**, 4968–4978.
18 M. Evangelisti, A. Candini, A. Ghirri, M. Affronte, E. K. Brechin and E. J. L. McInnes, Spin-enhanced magnetocaloric effect in molecular nanomagnets, *Appl. Phys. Lett.*, 2005, **87**, 1–4.
19 G. Brunet, R. Marin, M. J. Monk, U. Resch-Genger, D. A. Gálico, F. A. Sigoli, E. A. Suturina, E. Hemmer and M. Murugesu, Exploring the dual functionality of an ytterbium complex for luminescence thermometry and slow magnetic relaxation, *Chem. Sci.*, 2019, **10**, 6799–6808.
20 F. Cao, S. Wang, D. Li, S. Zeng, M. Niu, Y. Song and J. Dou, Family of Mixed 3d–4f Dimeric 14-Metallacrown-5 Compounds: Syntheses, Structures, and Magnetic Properties, *Inorg. Chem.*, 2013, **52**, 10747–10755.
21 E. M. Pineda, F. Tuna, Y. Z. Zheng, R. E. P. Winpenny and E. J. L. McInnes, Wells-Dawson cages as molecular refrigerants, *Inorg. Chem.*, 2013, **52**, 13702–13707.
22 S. K. Langley, N. F. Chilton, B. Moubaraki, T. Hooper, E. K. Brechin, M. Evangelisti and K. S. Murray, Molecular coolers: The case for [$Cu^{II}5Gd^{III}4$], *Chem. Sci.*, 2011, **2**, 1166–1169.
23 M. Evangelisti, O. Roubeau, E. Palacios, A. Camón, T. N. Hooper, E. K. Brechin and J. J. Alonso, Cryogenic magnetocaloric effect in a ferromagnetic molecular dimer, *Angew. Chem., Int. Ed.*, 2011, **50**, 6606–6609.
24 F. S. Guo, Y. C. Chen, L. L. Mao, W. Q. Lin, J. D. Leng, R. Tarasenko, M. Orendáč, J. Prokleška, V. Sechovský and M. L. Tong, Anion-templated assembly and magnetocaloric properties of a nanoscale {Gd38} cage versus a {Gd48} barrel, *Chem. – Eur. J.*, 2013, **19**, 14876–14885.
25 K. S. Pedersen, G. Lorusso, J. J. Morales, T. Weyhermüller, S. Piligkos, S. K. Singh, D. Larsen, M. Schau-Magnussen, G. Rajaraman, M. Evangelisti and J. Bendix, Fluoride-bridged {$Gd^{III}3M^{III}2$} (M=Cr, Fe, Ga) molecular magnetic refrigerants, *Angew. Chem., Int. Ed.*, 2014, **53**, 2394–2397.
26 Y. C. Chen, F. S. Guo, J. L. Liu, J. D. Leng, P. Vrábel, M. Orendáč, J. Prokleška, V. Sechovský and M. L. Tong, Switching of the magnetocaloric effect of MnII glycolate by water molecules, *Chem. – Eur. J.*, 2014, **20**, 3029–3035.
27 J. B. Peng, Q. C. Zhang, X. J. Kong, Y. Z. Zheng, Y. P. Ren, L. S. Long, R. B. Huang, L. S. Zheng and Z. Zheng, High-nuclearity 3d–4f clusters as enhanced magnetic coolers and molecular magnets, *J. Am. Chem. Soc.*, 2012, **134**, 3314–3317.
28 M. R. Azar, T. T. Boron, J. C. Lutter, C. I. Daly, K. A. Zegalia, R. Nimthong, G. M. Ferrence, M. Zeller, J. W. Kampf, V. L. Pecoraro and C. M. Zaleski, Controllable formation of heterotrimetallic coordination compounds: Systematically incorporating lanthanide and alkali metal ions into the manganese 12-metallacrown-4 framework, *Inorg. Chem.*, 2014, **53**, 1729–1742.
29 M. Ostrowska, Y. Toporivska, I. A. Golenya, S. Shova, I. O. Fritsky, V. L. Pecoraro and E. Gumienna-Kontecka, Explaining How α-Hydroxamate Ligands Control the Formation of Cu(II)-, Ni(II)-, and Zn(II)-Containing Metallacrowns, *Inorg. Chem.*, 2019, **58**, 16642–16659.
30 A. Lüpke, L. M. Carrella and E. Rentschler, Filling the gap in the metallacrown family: The 9-MC-3 chromium metallacrown, *Chem. – Eur. J.*, 2021, **27**, 4283–4286.
31 P. Happ and E. Rentschler, Enforcement of a high-spin ground state for the first 3d heterometallic 12-metallacrown-4 complex, *Dalton Trans.*, 2014, **43**, 15308–15312.
32 T. T. Boron, J. C. Lutter, C. I. Daly, C. Y. Chow, A. H. Davis, R. Nimthong, M. Zeller, J. W. Kampf, C. M. Zaleski, V. L. Pecoraro, A. Nimthong-Roldán, M. Zeller, J. W. Kampf, C. M. Zaleski and V. L. Pecoraro, The Nature of the Bridging Anion Controls the Single-Molecule Magnetic Properties of DyX4M 12-Metallacrown-4 Complexes, *Inorg. Chem.*, 2016, **55**, 10597–10607.
33 C. Y. Chow, R. R. R. Guillot, E. Rivière, J. W. Kampf, T. Mallah, V. L. Pecoraro, L. Vincent, A. Arbor and O. Cedex, Synthesis and Magnetic Characterization of Fe(III)-Based 9-Metallacrown-3 Complexes Which Exhibit

Magnetorefrigerant Properties, *Inorg. Chem.*, 2016, **55**, 10238–10247.

34 M. S. Lah, M. L. Kirk, W. Hatfield and V. L. Pecoraro, The tetranuclear cluster Fe^{III} [Fe^{III} (salicylhydroximato)(MeOH)(acetate)]$_3$ is an analogue of M^{3+} (9-crown-3), *J. Chem. Soc., Chem. Commun.*, 1989, 1606–1608.

35 C. Y. Chow, S. V. Eliseeva, E. R. Trivedi, T. N. Nguyen, J. W. Kampf, S. Petoud and V. L. Pecoraro, Ga^{3+}/Ln^{3+} Metallacrowns: A Promising Family of Highly Luminescent Lanthanide Complexes That Covers Visible and Near-Infrared Domains, *J. Am. Chem. Soc.*, 2016, **138**, 5100–5109.

36 B. Emerich, M. Smith, M. Zeller and C. M. Zaleski, Synthesis and Crystal Structure of $Mn^{II}(OAc)_2$[15-MC ^{III}Mn(N)shi-5] $(Im)_3(EtOH)_3$ (shi3– = salicylhydroximate, –OAc = acetate, Im = imidazole, and EtOH 5 ethanol), *J. Chem. Crystallogr.*, 2010, **40**, 769–777.

37 J. Jankolovits, C. M. Andolina, J. W. Kampf, K. N. Raymond and V. L. Pecoraro, Assembly of near-infrared luminescent lanthanide host(host-guest) complexes with a metallacrown sandwich motif, *Angew. Chem., Int. Ed.*, 2011, **50**, 9660–9664.

38 G. Mezei, C. M. Zaleski and V. L. Pecoraro, Structural and Functional Evolutions of Metallacrowns, *Chem. Rev.*, 2007, **107**, 4933–5003.

39 P. Happ, C. Plenk and E. Rentschler, 12-MC-4 metallacrowns as versatile tools for SMM research, *Coord. Chem. Rev.*, 2015, **289–290**, 238–260.

40 C. Plenk, J. Krause, M. Beck and E. Rentschler, Rational linkage of magnetic molecules using click chemistry, *Chem. Commun.*, 2015, **51**, 6524–6527.

41 A. B. Lago, J. Pasán, L. Cañadillas-Delgado, O. Fabelo, F. J. M. Casado, M. Julve, F. Lloret and C. Ruiz-Pérez, A three-dimensional copper(II) 12-metallacrown-4 complex with malonomonohydroxamic acid (H3mmh) as a ligand, *New J. Chem.*, 2011, **35**, 1817–1822.

42 C. McDonald, T. Whyte, S. M. Taylor, S. Sanz, E. K. Brechin, D. Gaynor and L. F. Jones, Progressive decoration of pentanuclear Cu(II) 12-metallacrown-4 nodes towards targeted 1- and 2D extended networks, *CrystEngComm*, 2013, **15**, 6672–6681.

43 Y. Song, J. C. Liu, Y. J. Liu, D. R. Zhu, J. Z. Zhuang and X. Z. You, Preparation, crystal structures and magnetic properties of 12-metallacrown-4 complexes with the donors on the organic periphery of molecule, *Inorg. Chim. Acta*, 2000, **305**, 135–142.

44 T. Lou, H. Yang, S. Zeng, D. Li and J. Dou, A New Family of Heterometallic Ln^{III}[12-MCFe^{III}N(shi)-4] Complexes: Syntheses, Structures and Magnetic Properties, *Crystals*, 2018, **8**, 229.

45 *CrysAlisPro 1.171.38.41, Rigaku Oxford Diffr*.

46 R. Americas, *CrystalClear Expert 2.0 r16*, Tokyo, Japan, 2004.

47 G. M. Sheldrick, Crystal structure refinement with SHELXL, *Acta Crystallogr., Sect. C: Struct. Chem.*, 2015, **71**, 3–8.

48 J. R. Travis, A. M. Smihosky, A. C. Kauffman, S. E. Ramstrom, A. J. Lewis, S. G. Nagy, R. E. Rheam, M. Zeller and C. M. Zaleski, Syntheses and Crystal Structures of Two Classes of Aluminum-Lanthanide-Sodium Heterotrimetallic 12-Metallacrown-4 Compounds: Individual Molecules and Dimers of Metallacrowns, *J. Chem. Crystallogr.*, 2020, DOI: 10.1007/s10870-020-00861-2.

49 E. V. Salerno, S. V. Eliseeva, B. L. Schneider, J. W. Kampf, S. Petoud and V. L. Pecoraro, Visible, Near-Infrared, and Dual-Range Luminescence Spanning the 4f Series Sensitized by a Gallium(III)/Lanthanide(III) Metallacrown Structure, *J. Phys. Chem. A*, 2020, **124**, 10550–10564.

50 A. B. Lago, J. Pasán, L. Cañadillas-Delgado, O. Fabelo, F. J. M. Casado, M. Julve, F. Lloret and C. Ruiz-Pérez, A three-dimensional copper(II) 12-metallacrown-4 complex with malonomonohydroxamic acid (H3mmh) as a ligand, *New J. Chem.*, 2011, **35**, 1817–1822.

51 C. Y. Chow, H. Bolvin, V. E. Campbell, R. Guillot, J. W. Kampf, W. Wernsdorfer, F. Gendron, J. Autschbach, V. L. Pecoraro and T. Mallah, Assessing the exchange coupling in binuclear lanthanide(III) complexes and the slow relaxation of the magnetization in the antiferromagnetically coupled Dy2 derivative, *Chem. Sci.*, 2015, **6**, 4148–4159.

52 D. P. Kessisoglou, J. Kampf and V. L. Pecoraro, Compositional and geometrical isomers of 15-metallacrowns-5 complexes, *Polyhedron*, 1994, **13**, 1379–1391.

53 T. Afrati, C. Dendrinou-Samara, C. M. Zaleski, J. W. Kampf, V. L. Pecoraro and D. P. Kessissoglou, Synthesis and structure of [18-MCCuII(N)pko-6]$^{6+}$: A new member of anion encapsulating metallamacrocyles, *Inorg. Chem. Commun.*, 2005, **8**, 1173–1176.

54 N. F. Chilton, R. P. Anderson, L. D. Turner, A. Soncini and K. S. Murray, PHI: A powerful new program for the analysis of anisotropic monomeric and exchange-coupled polynuclear d- and f-block complexes, *J. Comput. Chem.*, 2013, **34**, 1164–1175.

55 A. A. Athanasopoulou, L. M. Carrella and E. Rentschler, Slow relaxation of magnetization in a {Fe 6 Dy} complex deriving from a family of highly symmetric metallacryptands, *Dalton Trans.*, 2019, **48**, 4779–4783.

56 S. T. Liddle and J. Van Slageren, Improving f-element single molecule magnets, *Chem. Soc. Rev.*, 2015, **44**, 6655–6669.

57 P. Wang, S. Shannigrahi, N. L. Yakovlev and T. S. A. Hor, Facile self-assembly of intermetallic [Ni_2Gd_2] cubane aggregate for magnetic refrigeration, *Chem. – Asian J.*, 2013, **8**, 2943–2946.

58 Y. Z. Zheng, E. M. Pineda, M. Helliwell and R. E. P. Winpenny, Mn II-Gd III phosphonate cages with a large magnetocaloric effect, *Chem. – Eur. J.*, 2012, **18**, 4161–4165.

59 K. Wang, H.-H. Zou, Z.-L. Chen, Z. Zhang, W.-Y. Sun and F.-P. Liang, A series of 3D metal organic frameworks based on [24-MC-6] metallacrown clusters: structure, magnetic and luminescence properties, *Dalton Trans.*, 2014, **43**, 12989.

60 F. S. Guo, Y. C. Chen, J. L. Liu, J. D. Leng, Z. S. Meng, P. Vrábel, M. Orendáč and M. L. Tong, A large cryogenic

magnetocaloric effect exhibited at low field by a 3D ferromagnetically coupled Mn(II)–Gd(III) framework material, *Chem. Commun.*, 2012, **48**, 12219–12221.

61 K. Kambe, On the Paramagnetic Susceptibilities of Some Polynuclear Complex Salts, *J. Phys. Soc. Jpn.*, 1950, **5**, 48–51.

62 T. Mallah and A. Marvilliers, in *Magnetism: Molecules to Materials*, Wiley-VCH Verlag GmbH & Co. KGaA, Weinheim, Germany, 2003, pp. 189–226.

63 M. Jarenmark, M. Haukka, S. Demeshko, F. Tuczek, L. Zuppiroli, F. Meyer and E. Nordlander, Synthesis, characterization, and reactivity studies of heterodinuclear complexes modeling active sites in purple acid phospatases, *Inorg. Chem.*, 2011, **50**, 3866–3887.

64 P. Román, C. Guzmán-Miralles, A. Luque, J. I. Beitia, J. Cano, F. Lloret, M. Julve and S. Alvarez, Influence of the peripheral ligand atoms on the exchange interaction in oxalato-bridged nickel(II) complexes: An orbital model. Crystal structures and magnetic properties of (H3dien)2 [Ni2(ox)5]·12H_2O and [Ni2(dien)2(H_2O)2(ox)]Cl2, *Inorg. Chem.*, 1996, **35**, 3741–3751.

65 H. Astheimer and W. Haase, Direct theoretical ab initio calculations in exchange coupled copper(II) dimers: Influence of structural and chemical parameters in modeled copper dimers, *J. Chem. Phys.*, 1985, **85**, 1427–1432.

66 A. Scuiller, T. Mallah, M. Verdaguer, A. Nivorozhkin, J.-L. Tholence and P. Veillet, A rational route to high-spin molecules via hexacyanometalates: a new u-cyano $Cr^{III}Mn^{II}$6 heptanuclear complex with low-lying S = 27/2 ground state, *New J. Chem.*, 1996, **20**, 1.